Title: A Local Projection-Based Approach to Individual Tree Detection and 3-D Crown Delineation in Multistoried Coniferous Forests Using High-Density Airborne LiDAR Data.

This paper appears in: IEEE Transactions on Geoscience and Remote Sensing

Date of Publication: 10 September 2018

Author(s): Aravind Harikumar, Francesca Bovolo, Lorenzo Bruzzone

Volume:

Page(s): 1 - 15

DOI: 10.1109/TGRS.2018.2865014

A Local Projection based Approach to Individual Tree Detection and 3D Crown Delineation in Multistoried Coniferous Forests using High Density Airborne LiDAR Data

Aravind Harikumar, *Student Member, IEEE,* Francesca Bovolo, *Senior Member, IEEE,* and Lorenzo Bruzzone, *Fellow, IEEE*

***Abstract*—Accurate crown detection and delineation of dominant and subdominant trees is crucial for accurate inventorying of forests at the individual tree level. State-of-the-art tree detection and crown delineation methods have good performance mostly with dominant trees, whereas exhibits a reduced accuracy when dealing with subdominant trees. In this paper, we propose a novel approach to accurately detect and delineate both dominant and subdominant tree crowns in conifer-dominated multistoried forests using small footprint high density airborne LiDAR data. Here, 3D candidate cloud segments delineated using a CHM segmentation technique are projected onto a novel 3D space where both dominant and subdominant tree crowns can be accurately detected and delineated. Tree crowns are detected using 2D features derived from the projected data. The delineation of crown is performed at the voxel level with the help of both the 2D features, and 3D texture information derived from the cloud segment. The texture information is modeled by using 3D Grey Level Co-occurrence Matrix (GLCM). The performance evaluation was done on a set of six circular plots for which reference data are available. The high detection and delineation accuracies obtained over the state of the art prove the performance of the proposed method.**

***Index Terms*—Tree Top Detection, 3D Tree Crown Delineation, Light Detection and Ranging (LiDAR), Forest, Airborne Laser Scanner (ALS).**

I. INTRODUCTION

Accurate forest inventory and biophysical parameter estimations are essential for a variety of forest characterization and management activities including forest ecosystem modeling, forest fire models, timber and wildlife habitat management [1]. Light Detection and Ranging (LiDAR) remote sensing is a popular technique used to capture three dimensional (3D) data by using highly directed laser beams. In the case of forests, the laser beam (or part of it) gets reflected from different canopy layers and hence captures the 3D vertical profile information. In multistoried forests, these properties of laser allow LiDAR to capture information about both dominant and subdominant trees. In this context of multistoried forests, dominant trees are those with the tallest and often widest crowns in their local neighborhood, and hence have the maximum visibility in the canopy layer. While, the subdominant ones are smaller trees that are found close to dominant ones, with smaller crown size, and hence are invisible/partially visible at the canopy layer (Fig. 1). Effective subdominant tree detection and delineation are important as this category of trees: a) contribute largely to the forest biomass, b) are useful for accurate forest environment modeling, and c) represent young trees.

Several forest inventory measures such as the tree height [2], the crown cover, the basal area, and forest parameter estimates such as the biomass, the leaf area index, and the Diameter at Breast Height (DBH), can be estimated directly or indirectly from the 3D data. Most operational LiDAR data based inventories are performed using area/stand based techniques. They use samples collected from small circular or square forest plots to estimate forest biophysical parameters using statistical methods. However, a single stand can contain trees from multiple classes and/or species having different characteristics, and thus prior information such as stem number and tree species is needed for a better prediction of the stand parameters [3]. Whatsoever, the inherent coarseness in the analysis results in a reduced accuracy of the parameter estimates. These methods are preferred mostly when the variables to be estimated apply to the whole range of variation in an area [4]. For forest management practices requiring an accurate estimation of local biophysical parameters (e.g., forest fire prediction analysis), the Individual Tree Level (ITC) inventorying is preferred over the area based ones, [2], [5], [6]. In general, the performance of ITC is maximum mostly in mature forests [7]. However, individual tree level inventorying requires accurate detection and delineation of tree crowns, as they are critical factors that affect the performance of forest parameter estimation [3], and tree species classification [8]. In the framework of forest analysis, the tree detection refers to identifying the location of the tree, while the crown delineation refers to delineating the tree crown in 3D. In individual tree level analysis, the crown detection step usually precedes the crown delineation. Both tree detection and crown delineation are challenging in multistoried forests as: a) the crowns of shorter/smaller (subdominant) trees are often obstructed by taller (dominant) ones, b) the trees are often proximal to one another and hence crowns overlap, and c) the LiDAR point density decreases

Aravind Harikumar and Lorenzo Bruzzone are with the Department of Information Engineering and Computer science, Trento, Italy. E-mail: (see aravind.harikumar@unitn.it).

Aravind Harikumar and Francesca Bovolo are with Fondazione Bruno Kessler, Trento, Italy.

Manuscript received January 16, 2018

as we move from the top of a canopy towards the bottom. These situations often make it difficult to accurately detect and delineate both dominant and subdominant trees [9], [10].

Canopy Height Model (CHM) [11] based approaches are conventionality and widely used for crown detection and delineation mainly due to their simplicity. Crown delineation is performed by segmenting CHM, based on tree tops detected using local maxima [11] or level set [12] method. The rasterization artefacts in the CHM combined with the irregularities in crown shape, affects the crown detection and delineation accuracies, and hence are smoothened out using a Gaussian low-pass filter [13], [14]. Thus, optimal smoothing parameters are critical for accurate tree detection and delineation. These parameters are often estimated by modeling topological relation of crown segments with one another [15], rule based splitting and merging of crown segments [16], or methods based on local extrema calculated from combinations of normalised scale invariant CHM derivatives [13]. In case of mixed/multilayered forests with variable crown size (and thus no single optimal resolution), adaptively varying filter window size improved crown detection accuracy [17], [11]. Alternatively, multistage object-based approach to tree delineation using region growing approaches are also developed [18], [19]. However, the approach demands an overhead of fine tuning of the search-radius/merge-conditions for optimal results, due to the effect of CHM smoothing and poor window size selection. CHM based treetop detection techniques when used singlehandedly can detect and delineate most of the dominant crowns, but often fail to detect subdominant tree crowns since they are: a) partially (or completely) obstructed by dominant tree crowns, and b) less prominent in the CHM (see Fig. 1). Subdominant trees are often misdetected as a part of a dominant tree crown resulting in an under-/over-estimation of parameters like biomass.

Considering the limited ability of CHM in accurately representing tree crowns, in particular the subdominant ones, an increasing trend of exploiting 3D information along the height profile is observed in the literature. Exploiting the full potential of LiDAR data, several studies delineate tree crowns directly in the point cloud space. The simple k-means clustering applied to normalized point cloud, with seed points identified through CHM segmentation, highlighted the possibility of an accurate 3D crown delineation [20]. In an attempt to improve delineation of trees with irregular canopy size, Lee et al. applied region growing for generating initial 3D segments, and performed agglomerative clustering to accurately segment individual tree crowns [21]. In some studies, the horizontal spacing between tree crowns [22] and the variation in vertical density profiles of CHM segments [23] have been exploited to delineate tree crowns. Methods performing 3D layerwise analysis on tree point cloud to mitigate the problem of reduced point density in the understory also exist in the literature [24]. For example, layer-wise segments derived through clustering of the point cloud segments in every layer are stacked together and inspected for overlap to detect potential tree crowns [25]. Voxel-based approaches also exist in the literature. For example, Wang et al. delineated tree crowns using cluster features derived at every horizontal layer along the tree height. Each layer is divided into cells, and the points within the each study cell are resampled into the local voxel space (within), to derive the projection images [26]. In a more recently proposed voxel-based approach, the complementary information derived from the tree top and the stem location is exploited for 3D tree crown delineation [27]. In a comparison on crown delineation methods performed on the same dataset, the accuracy varied from study to study from 25% to 90% [28]. The results prove that the accuracy is highly influenced by the crown delineation method. Forest type also impacts on delineation accuracy [29]. It has been inferred that high stand density and large forest heterogeneity have adverse effects on delineation accuracy [28]. In any case, many studies agree that state-of-the-art methods are lacking in the ability to detect and delineate subdominant trees [25]. [28], [30], [29].

Wang et al. proposed a hierarchical morphological approach to 2D crown data, derived from voxel layers analysis along the forest vertical profile, to delineate dominant and subdominant crowns in the 3D space [31]. Vega et al., proposed a multi-scale segmentation at the point level followed by a multi-criteria analysis of the segments for accurate crown localization and delineation. However, the accuracy associated with the subdominant tree detection is low mainly due to poor point density below the canopy layer [32]. In a bottom-up approach to detect and delineate tree crowns, Lu et al., first extracted tree trunks by exploiting the intensity difference between trunk and other parts of the tree, and assigning the remaining points to the trunk clusters based on a set of proximity rules (with respect to stem) [33]. Among studies using full waveform LiDAR data, [34], the ones based on ellipsoidal k-means clustering proved to provide good accuracies in multilayered forest. Here, the cluster centers of dominant trees are obtained from the CHM segments, while that of the subdominant trees are obtained in an iterative way using uniform seed placement which however often causes inaccuracies [35]. In a more recent attempt, Paris et al. delineated dominant and subdominant tree crowns by a radial-sector-wise analysis of crown vertical profile [36]. However, the method relies only on the crown boundary at the canopy layer to delineate crown, and hence does not fully exploit the 3D information in the data. Statistical approaches to estimate tree count are also proposed. For example, Maltamo et al. used a theoretical distribution to predict the stem number and the stem diameter of subdominant trees which are not visible in the canopy layer. The parameters of the distribution were calculated from a truncated diameter distribution of dominant trees [37]. With a similar objective, but under the assumption that the relative height of trees in a homogeneous Poisson stand determines the probability of observing them from the air, some authors estimated the subdominant stem count [38],[39], and predicted stem-diameter distribution without the knowledge of tree position [40]. Prior information of tree shape when used in the MAP estimation of the position, the size, and the crown shape also improves tree detection accuracy [41]. Nonetheless, statistical modeling of tree level parameters can be useful for: a) estimating the understory biophysical parameter in case of low point density, and b) correcting errors in the crown level parameters derived from the pure ITC technique.

Most of the state-of-the-art 2D and 3D single tree detection and delineation algorithms work efficiently mostly in the case of dominant trees, but show reduced performance with subdominant trees, especially in dense multistoried forests [32], [36]. It is also worth noting that the errors in detecting tree crowns are very likely to affect the accuracy of any downstream operation like crown delineation. However, methods that can accurately detect both dominant and subdominant trees using high density airborne LiDAR data are lacking in the literature. Thus, the major objectives of the paper are: a) to develop an automatic technique for dominant and subdominant tree crown detection in multistoried coniferous forest with minimal omission and commission errors, and b) to accurately delineate the detected dominant and subdominant tree crowns.

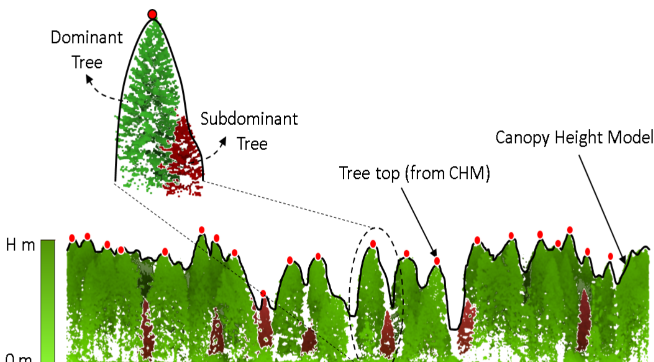

Fig. 1: CHM based tree detection and crown delineation. The dominant trees and Subdominant trees are shown in green and red, respectively.

II. Proposed Tree Detection and Delineation Method

In this paper, we propose a novel method for detecting and delineating both dominant and subdominant trees in a multistoried coniferous forest by combining 2D and 3D information derived from LiDAR data. Here, the focus is on coniferous forests as: 1) they constitute close to 80% of the European forest, and 2) they are important from both economic and ecological point of view. 3D candidiate tree crowns are extracted from the point cloud based on CHM segment boundaries extracted using a state-of-the-art technique. We reasonably assume that each 3D segment (which is henceforth referred as the 3D candidate segment) contains one dominant tree crown only, however, may contain a number of subdominant tree crowns. All LiDAR points in a 3D candidate segment are then projected onto a novel 3D Euclidean space, where detection and delineation of dominant and subdominant tree crowns are performed. The high level block scheme of the proposed method is shown in Fig. 2.

A. CHM segmentation

Let $P = \{p_i \in R^3, i = 1, 2, ..., N\}$ be the set of N LiDAR points in the input point cloud. $T_{CHM} = \{t_j \in R^3, j = 1, 2, ..., T\}$ is the set of 3D tree top locations, where T is the total number of tree tops detected by the level set method [12] applied to the CHM. Segmentation is performed on the CHM by using the marker-controlled compact watershed algorithm [42] with T_{CHM} as seeds. The compactness of segments is controlled using $q \in [0, \inf]$ [42]. Each CHM segment $C_i(i = 1, 2, 3..., T)$ corresponds to the 2D boundaries of a 3D candidate segment with one dominant tree and $S_i(i = 0, 1, 2, 3..., S)$ possible subdominant trees. The section of the 3D point cloud corresponding to individual CHM segments (i.e., 3D candidate segment) is extracted and analysed for: a) detecting the S_i subdominant tree crowns, and b) accurately delineating the dominant, and the S_i subdominant tree crowns.

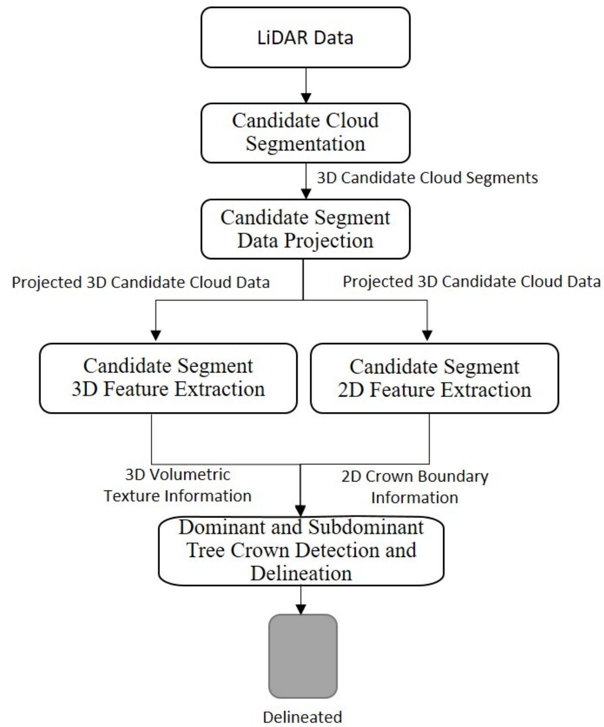

Fig. 2: Block scheme of the proposed crown detection and delineation approach.

B. Data projection

Analyzing the 3D candidate segments to accurately detect and delineate tree crowns in the original 3D Euclidean space is challenging as: a) the subdominant trees have smaller crowns, and are often close to the dominant ones, thus making it difficult to identify and delineate them; b) there is no or minimal difference in the crown-structural/volumetric-textural properties of a dominant tree and any proximal subdominant one; This makes it difficult to directly distinguish them using structural information in LiDAR data. Thus, we develop a technique that transforms the 3D candidate segment such that: a) smaller trees in it can be detected independently on their size and/or proximity to the dominant one; and b) a volumetric structure/textural modification is induced on the dominant tree crown without affecting its local branch structure, and any subdominant tree structure.

For each 3D candidate segment, we consider the neighborhood spanned by a cylinder with the axis along the dominant tree stem direction, and the radius r as the distance of the point farthest from the stem axis, and measured in a direction perpendicular to it. Here, the dominant tree stem is assumed to be vertically below the highest point $p_v = [x_v, y_v, z_v]$ in the 3D candidate segment. Any LiDAR point $p_i = [x_i, y_i, z_i]$ within the cylinder can then be uniquely projected into the novel space, spanned by the basis variables d, l, and z, using the projection equations (1), (2), and (3), which are designed to satisfy the transformation requirements.

$$d = \sqrt{(x_v - x_i)^2 + (y_v - y_i)^2} \tag{1}$$

$$l = 2\pi r\theta \tag{2}$$

$$z = z \tag{3}$$

where, $\{x_v,y_v\}$ and $\{x_i,y_i\}$ are the set of horizontal spatial coordinates of p_v and p_i, respectively. Here, d is the shortest distance between a LiDAR point p_i and the stem, l is the length of the arc with radius r, θ is the smallest angle between the p_i and the reference plane L_r, and z is the height of a point from the X-Y plane [43]. Interestingly, the transformation is equivalent to rolling out the space inside a solid cylinder into a cuboidal space (Fig. 3). It is worth noting that the transformation increases the distance between a pair of points (i.e., stretches the space) nearer to the axis of the cylinder, than to those located farther away from the axis. The amount of stretching is controlled by r; a larger r causes more stretching than a smaller r. In the case of conifers, branches grow outward from the central stem in directions nearly perpendicular to it. Thus, when the opening is performed along the stem of the dominant conifer, the section of every branch closer to the stem are pulled apart more than the section further away (see Fig. 3a-3c). It is worth mentioning that, in the projected space, the branches seem to emerge from a plane rather than a line (i.e., stem). This adds up as an advantage of the projection, allowing the entire 3D candidate segment to be visualized and analyzed from a single point perspective (Fig. 3c).

In the proposed transformation, the negative direction of L_r decides the vertical section where the cylinder is opened. L_r is selected such that it does not cross any subdominant tree crown. This is because, any subdominant tree, with part of the crown falling on either side of L_r (in the original space) is ripped apart to the either side of the rectangular cuboid (in the projected space). This undesirable situation leads to overestimation of subdominant tree count, hence reducing the crown delineation performance. Accordingly, we propose a Principal Component Analysis (PCA) based method which uses only the x and y components of the data for identifying the optimal reference plane direction. The assumption here is that conifers have a near-symmetrical crown, i.e., the spread of crown around the stem is near-symmetrical. However, the presence of subdominant trees disrupts this symmetry, and results in: a) data points further away from the main crown; and b) localized increase of point density (due to greater biomass per unit volume). In both the symmetry disrupting situations, the first principal component ($PC1$) is directed towards the subdominant trees, while the second principal component ($PC2$) points in an orthogonal direction. We choose L_r to be in the direction opposite to the resultant of PC1 and PC2, as it is very unlikely for that plane to pass through any of the subdominant tree point cloud even in complex situations where more than one subdominant tree exists in a 3D candidate segment. Fig. 4a shows an ideal 3D candidate segment containing one subdominant tree while Fig. 4e shows four subdominant trees near the dominant one. It can be observed that opening the point cloud along L_r derived as above, does not divide/rip apart the subdominant tree, in both the situations.

We also use the PCA analysis for detecting the presence of subdominant trees in a 3D candidate segment (as some 3D candidate segments may not have subdominant trees.) Let d_{min} and d_{max} be the distance of the points in the cloud that is maximally away from the stem in the direction of L_r and PC1, respectively. We identify these points by: a) fitting a maximally compact 2D convex hull on the x and y coordinate data of the point cloud, and b) finding the boundary points that are closest to, the line connecting the treetop point and its intersection in the convex hull boundary (in the respective direction). We consider the ratio of $\frac{d_{min}}{d_{max}}$ as an indicator of the presence of subdominant trees. A ratio close to 1 means that the distances in the two directions are similar, and hence the absence of a subdominant tree is assumed. Smaller ratios mean that the distances in the two directions are highly unequal, and hence refers to the presence of subdominant trees in the direction of PC1. Further analysis using data transformation is performed on 3D candidate segments for which the presence of subdominant trees is detected. The data transformation is advantageous for differentiating the dominant from subdominant tree crowns as it: a) deforms mostly the shape of the dominant tree crown, while maintaining the local crown structure; b) does not (or minimally) deforms the subdominant tree crowns; and c) allows observing the points associated with all the dominant tree branches from a single-point perspective. Fig. 4 shows the original and projected 3D data corresponding to an example candidate tree CHM segment, for simple (i.e., with 1 subdominant tree) and complex (i.e., with 4 subdominant trees) situations. The red boundary line in Fig. 4a,4e represents the CHM segment boundaries.

C. Candidate Segment 3D Feature Extraction

We perform the texture analysis in the transformed space at the voxel level, where the optimal voxel size is obtained by using a semivariogram analysis. The sill location in a semivariogram corresponds to the distance beyond which the correlation is minimum, and hence the distance at the sill is taken as the optimal voxel dimension. It is worth recalling here that the projection operation is equivalent to rolling out the space inside a solid cylinder (enclosing the 3D candidate segment data) placed along the stem of the dominant tree (Fig. 3). It should be noted that the intermediate stage (Fig.

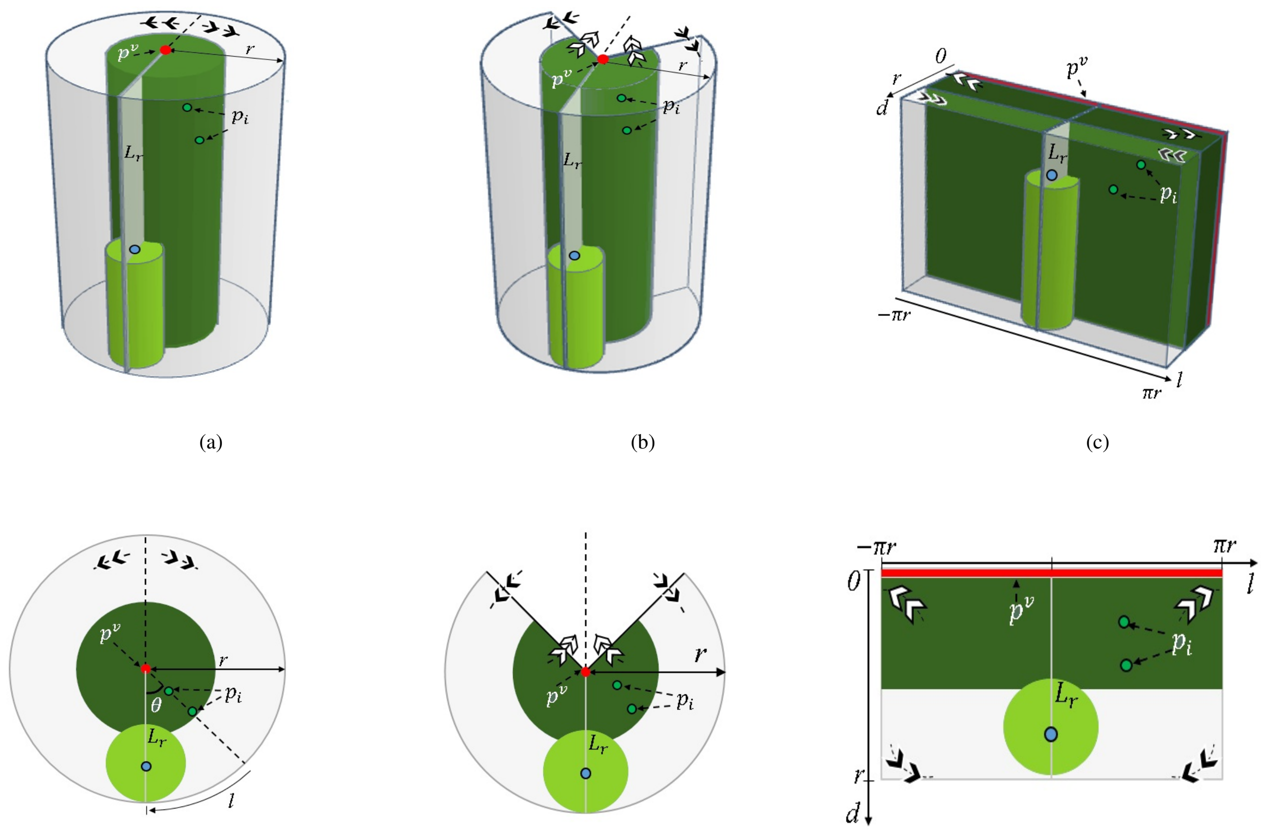

(a) (b) (c)

(d) (e) (f)

Fig. 3: Perspective and top view of solid cylinder placement on the original point cloud space (a,d), cylinder roll-out (b,e), and projected space (c,f).

3b,3e) is shown only to help visualize the spatial relationship between the initial and final states of the data. The rolling out affects mostly the dominant tree data, while the structure of subdominant trees is preserved. In the projected space, the branches of the dominant tree appear to grown straight up from the background plane, while the subdominant trees have their branches growing out from the respective stem locations. This induces a change in volumetric texture properties of the dominant tree crown, while maintaining the texture of the subdominant tree crowns. We exploit this variation in texture properties to delineate dominant and subdominant trees in the projected point cloud data.

In this paper, we use the Grey Level Co-occurrence Matrix (GLCM) texture features calculated on the number of points in each voxel. By considering the number of voxel-pairs with similar point count in a particular direction and within a fixed neighborhood, 3D GLCM is derived and used to extract voxel level texture information. Hence, for every voxel cell and a direction, a GLCM matrix is generated. Branches in the projected space often have slightly different vertical and horizontal tilts, resulting in directional variation in the local structure/texture. Thus, we derive GLCM matrices for 13 different directions, and averaged element-wise to get a single GLCM matrix [44]. In order to quantify texture variations from each averaged GLCM matrix, four Haralick texture features including energy, correlation, contrast, and homogeneity are calculated [45]. Although the feature extraction can also be performed on GLCM matrices generated with different neighborhood size and voxel distance, we restrict our analysis to the first order neighborhood and unit distance, respectively.

D. Candidate Segment 2D Feature Extraction and Boundary Detection

The l and z dimensions of each data point provide information about its position with respect to L_r, while d gives information about the distance of a point from the dominant tree stem. A 2D representation of the spatial variation in d on the $l-z$ plane helps to detect and delineate dominant and subdominant trees. The 3D data can be converted to a 2D representation by forming a square grid which spans the $l-z$ plane, and assigning values to each grid cell by selecting the largest d value falling within the respective cell. The grid size is chosen to be the same as that of the semivariogram. We refer to the 2D representation as the Candidate Segment Surface Model (CSSM), as it essentially models the spatial variation of the maximum d values in the projected data. It is worth noting that the CSSM generation process is similar to that of the forest CHM in the original point cloud space, where the

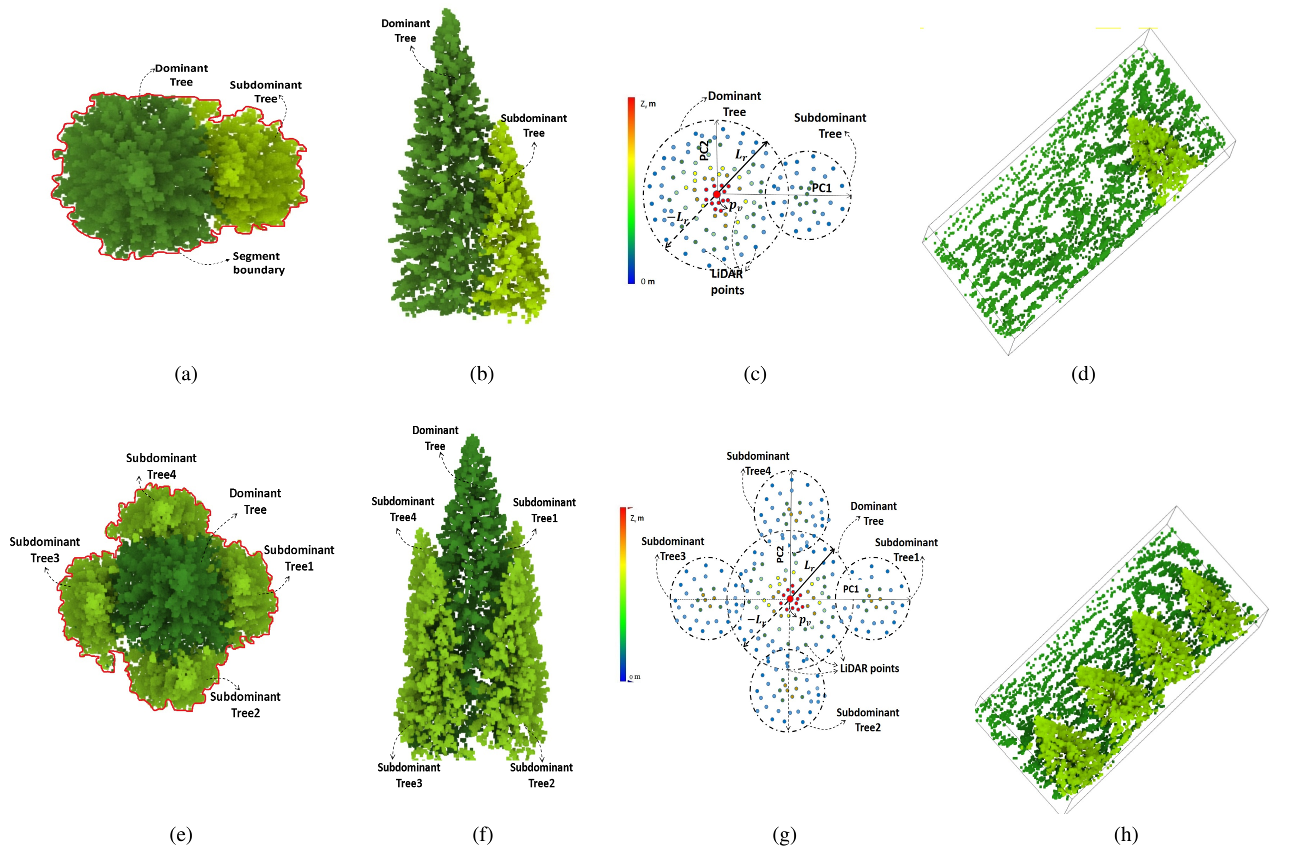

Fig. 4: Subdominant tree growth scenarios: (a,e) the top view, (b,f) the side view, (c,g) the reference plane direction estimation, and (d,h) the projected point cloud. Cases with one (simple case), and four (complex case) subdominant trees are illustrated.

points with the maximum d values in each grid determine the exterior crown boundary instead. In general subdominant tree crowns, and thus the corresponding data points, exist farther from the stem of the dominant tree. As a result, the sections of CSSM representing the subdominant tree crowns have relatively larger d values compared to the dominant crown sections. The presence of subdominant trees often results in an increase in biomass volume (due to leaves, branches, and stem) and in turn causes a local increase in LiDAR point density. It is worth recollecting here that the subdominant tree point cloud within the 3D candidate segment mostly remains unaffected by the projection, while the dominant tree point cloud (within the 3D candidate segment) is rolled out along its stem axis. As a result, the point density of the region spanned by dominant tree crown in the (l-z) plane is lowered by approximately half, while the density of the subdominant tree remains unaffected (Fig. 4b,4d). By using the number of LiDAR points (rather than the largest d within a grid) as the selected parameter, one can generate the Candidate Segment Density Model (CSDM).

We detect subdominant trees crown boundary by performing the simple k-means segmentation on the Gaussian smoothed candidate segment features. The number of clusters is set to 2 to extract the dominant, and the subdominant crown segments. We identify the foreground cluster (which represents the subdominant crowns) based on the mean values of pixels belonging to the cluster in the CSSM and CDSM. A larger mean value is found in the cluster containing the subdominant tree(s), and is selected as the foreground cluster. Each foreground segment boundary closely follows the subdominant tree crown boundary in the $l - z$ plane. For each segment boundary the local maximum in its upper half corresponds to the subdominant tree top, while the maximum extent of the segment along the l axis represents the maximum crown radius. Sometimes the segments of multiple subdominant trees merge due to crown proximity, creating a merged segment. However, in any case, the merge happens mostly below a certain crown height (due to the tapered-top characteristic shape of conifers), hence creating a local minimum between two local maxima. In these situations, the position of the local minima on either side of the local maximum determines the crown span. We implement this analysis by: a) identifying the upper half (along z) of the boundary segment, and assigning minimum values to remaining sections along l not spanned by the segment boundary; b) fitting a curve passing through all the upper envelope points; and c) detecting the local maximum/maxima and local minimum/minima of the fitted curve. This information about the position of the local maximum combined with the two local minima on its both sides, is used to create an approximate shape of the subdominant tree. In our case, we use an elliptical shape, as it can model tree crowns effectively. The major axis length (a_e) and minor axis length (b_e) of the ellipse are assumed to be the local maximum height (i.e., the subdominant tree height), and the horizontal distance between the local minima on either sides of the local maximum (i.e., the subdominant tree crown width). The center of the ellipse is placed at half the height of a local maximum. The ellipse is used as an input to accurate detection and delineation of the 3D tree crown.

E. Dominant and Subdominant Tree Crown Detection and Delineation

We achieve crown delineation in the projected 3D space by performing segmentation of the voxels based on the texture properties. The segmentation is performed on the so-called multispectral scalar image which is obtained by pixel by pixel averaging of the gradient image obtained against the individual texture features [46]. Whatsoever, the point density within the tree crown in the original space decreases from the exterior of the crown towards the stem, and also from the top of the crown towards the bottom. Consequently, in the projected space, the point density decreases in the direction of the positive d axis and decreases in the direction of decreasing z axis. In other words, the point density varies within a tree crown. This can affect the performance of most volumetric segmentation (i.e., 3D segmentation) techniques. However, the point density variation within a horizontal layer along d is small. Thus, we perform segmentation on the interpolated image of the layer-wise texture data. The number of layers along d is defined by the voxel size.

All voxels whose centers are located below a threshold $d_t = \frac{d_{min} * r}{d_{max}}$ belong to the dominant crown, While the remaining voxels contain the subdominant crown(s). Individual subdominant crown(s) is extracted at the voxel level by stacking the group of all structurally similar voxel cells from different d layers. For each tree, segments from all d layers that has the major portion of its area falling within the respective elliptical boundary (derived from 2D analysis of candidate segment in Sec. II-D) are stacked. We perform multivariate marker-controlled watershed algorithm [46] on interpolated texture feature maps to identify such segments in individual d layers. A spatial Gaussian filtering is applied to each texture layer in order to smoothen out any local irregularity and to avoid oversegmentation. The stacked voxel segments define the 3D crown of the subdominant tree(s) in the projected space. Every data point inside the projected segment is then assigned to one of the voxel cells, based on the proximity of a point to the center of a voxel cell. The index of points belonging to the individual stacked-voxel segments define the point cloud of a tree in the original space. Any unassigned point is assigned to one of the tree cloud segments based on proximity.

However, CHM based segmentation may result in a subdominant tree crown being split between 3D candidate segments (Fig. 5a) (i.e., section of the subdominant tree crown is allocated to different proximal 3D candidate segments) and hence will be detected and delineated as separate trees in the respective 3D candidate segments (Fig. 5b). This results in an overestimation of subdominant tree count, and an underestimation of the crown size. To address this issue, we merge subdominant tree clusters if they have: a) similar crown boundary parameters on data points in the G most external d slices of the 3D candidate segment. These are the ones corresponding to the largest d values. Here we consider $G = 2$ to include enough points for crown segment boundary estimation (i.e., $\cup(d_D, d_{D-1})$ (Fig. 5c). Elliptical crown boundary parameters a_e and b_e are calculated as in Section II-D and used for similarity estimation; and b) the Euclidean distance p_S^t between the highest point in the respective slices is small. For each subdominant tree cluster, we represent these parameter values as a 3D vector $t_d = [a_e \ b_e \ p_s^t]$. Clusters pairs with the Euclidean difference between corresponding t_d vectors less than a threshold are merged. It is worth noting that the proposed split-crown merging technique works also for complex situations where a crown is split into more than 2 parts.

We consider the horizontal position of the highest point in the delineated point cloud as the location of the tree. The maximum radius of a delineated crown is calculated as the perpendicular distance of the point that is maximally away from the line connecting the highest point in the subdominant tree segment and its projection on the ground.

III. Experiments and Results

A. Study Area, Dataset

The study area is a multistoried coniferous forest in the southern Italian Alps, in the municipality of Pellizzano located in the Trentino region in Italy. The altitude of this mountainous terrain ranges from 900 m to 2000m above sea level. The area has an extent of 3200 ha with the geographic center point of $46^0 17' 31.00''$ N and $10^0 45' 56.49''$ E. High density LiDAR data were acquired between 7th and 9th of September 2012 using a Riegl MS-Q680 sensor. The acquisition was performed from an airborne platform flying at an average height of 660m above ground level with a speed of around 180km/hr. The pulse repetition frequency was 400 KHz and recorded a maximum of four returns for each laser pulse fired. The major tree species include the Norway spruce (Picea abies), the European Larch (Larix decidua), and the Silver Fir (Abies alba).

The experiments were conducted on a set of 6 plots containing both dominant and subdominant trees. The radius of each plot is 25m. The plot centers were measured using a survey grade differential GPS, which provided a root mean square error of 0.25m in a separate validation. The position of trees within a plot was measured with respect to the center of the plot using an ultrasound instrument with high measurement accuracy of 0.25m. The height, the DBH (at 1.3m above the ground), and the species are also available from an in situ survey. The height of individual trees was estimated using regression models (4) based on a set of reference trees for which height is also known.

$$h_i = \alpha_0 + \alpha_1 ln(DBH_i) + \epsilon \tag{4}$$

where h_i is the height of i_{th} tree, DBH_i is the DBH of the i_{th} tree, and ϵ is the error term in the regression function. The α_0 and α_1 are regression parameters [35]. Regression models were derived for each species in the dataset separately. The

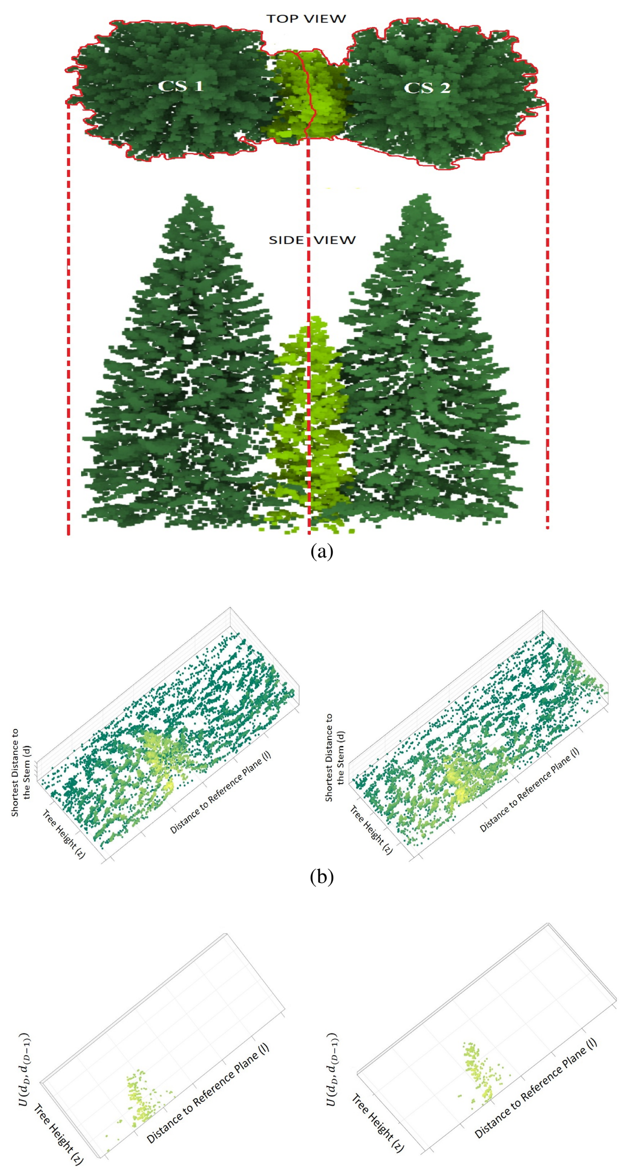

(a)

(b)

(c)

Fig. 5: (a) Top and side view of two proximal 3D candidate segments (CS1 and CS2) with a split subdominant tree crown, and (b) shows the corresponding projected 3D candidate segment, and (c) $\cup(d_D, d_{D-1})$.

estimated height is used for correcting/rectifying the positional errors of trees [47]. Each delineated tree i derived using the proposed and the state-of-the-art methods is linked to a tree j in the reference data based on the distance d_{ij} (5). For the case with multiple trees satisfying the distance criteria, the most proximal tree is linked to the reference data. Only clusters which fall completely within the boundary of the plot are included for the validation. However, a few trees near the plot boundary which satisfy the inclusion condition are not used in the validation due to lack of field data, i.e., such cases counted to a total of 7 trees.

$$d_{ij} = \sqrt{(r_{xy}^2 + (r_z/3)^2)} \tag{5}$$

where the r_z is the vertical distance, and r_{xy} is the horizontal distance between the highest point in the delineated tree i and the nearest reference tree j. A delineated tree is linked to a reference tree only if d_{ij} is less than 1.5m + 2DBH, in order to allow for positioning and height errors or else is considered as a Commission Error (CE) [35]. The DBH estimation for every tree is performed using a model that employs the tree height and the crown diameter as the independent variables (6).

$$\sqrt{DBH_i} = b_0 + b_1\sqrt{h_i} + b_2\sqrt{d_i} + \epsilon \tag{6}$$

where DBH_i is the estimated DBH (in mm) of the i^{th} tree, and h_i and d_i are the tree height (in dm) and the crown diameter (in dm), respectively. The b_0, b_1 and b_2 are model parameters. The coefficients of the model used for Norway spruce are $b_0 = -3.524$, $b_1 = 0.729$ and $b_2 = 1.345$, whereas for other species the model coefficients are $b_0 = -3.733$, $b_1 = 0.807$, and $b_2 = 1.144$ [48].

TABLE I: Statistics of the structural characteristics of the trees in the dataset considered for automatic segmentation.

Plot	#Trees	DBH (cm)		Crown Radius (m)	
		Range	Mean	Range	Mean
H1	40	9.0 - 76.0	39.6	1.3 - 7.0	3.7
H2	32	9.0 - 78.0	44.0	2.0 - 7.5	5.2
H3	30	16.0 - 77.0	35.5	2.6 - 7.8	4.4
H4	25	20.0 - 92.0	53.4	3.7 - 7.7	5.8
H5	45	25.0 - 67.0	35.1	2.1 - 6.9	4.2
H6	38	9.1 - 81.0	33.6	1.3 - 6.8	3.6

B. Experimental Results and Discussion

The performance quantification was conducted on the 6 plots to investigate the operational effectiveness of the proposed method. The dominant tree tops detected using the level set algorithm are used as the markers for the marker-controlled compact watershed segmentation on CHM, which in turn is used to delineate 3D candidate segments. The compactness parameter q is set to 1 as it was found to be optimal for minimizing the over-segmentation errors [42]. The spatial resolution of the CHM was chosen on the basis of the average number of LiDAR points/m^2, while the 2D Gaussian filter parameters were tuned to minimize false peaks in the CHM. In our case, the CHM resolution and the Gaussian filter size are selected to be 0.25 and 5 x 5, respectively. Fig. 8 shows the watershed segments for plot H1. The watershed segment boundaries are used to generate the 3D candidate segments, i.e., all points within a CHM boundary are assigned to the respective segment. However, CHM smoothening results in points to remain unassigned near/outside the CHM boundaries. Thus, unassigned points are assigned to the nearest candidate segment. Fig. 10 shows the candidate tree segments for four scenarios with one, and four subdominant trees, respectively. Each candidate data segment is then projected into the proposed space to detect subdominant trees. Fig. 7a and Fig. 7b show the 3D visualization of the projected data with and without a subdominant tree, respectively. Here, large d values associated with the subdominant trees are shown in shades of red, while the low values correspond to the

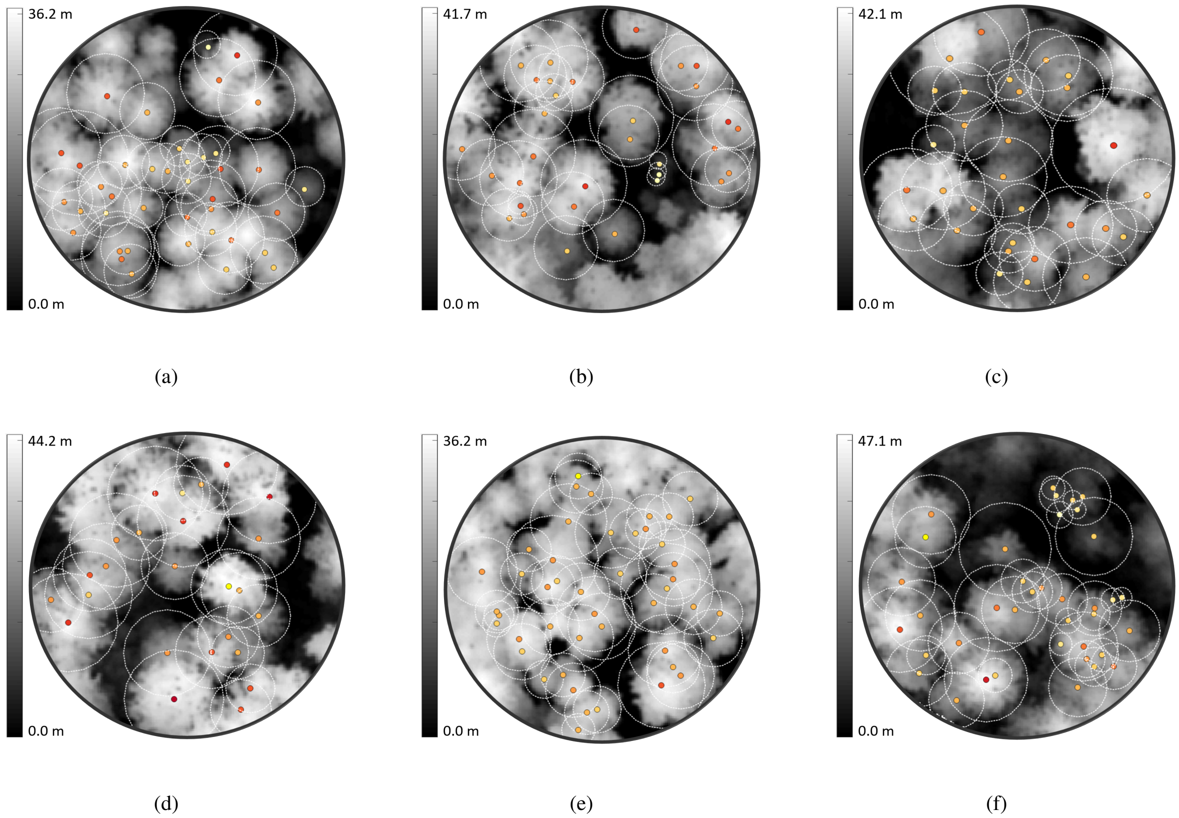

Fig. 6: (a)-(f) High density LiDAR data CHM representations of the plots with individual tree tops (in red) and respective maximum crown extents (white dotted circles). The points represent the crown center, and is colored based on the DBH value. Small to large DBHs are represented in shades from yellow to red.

background/dominant tree crown points, and appears in shades of yellow and green.

The projected space is divided into voxels. The optimal voxel size is obtained against the range of an exponentially fitted semivariogram. However, the range is set to 0.5m for the case in which semivariance does not saturate. Fig. 11(a-d) show the projected point cloud of dominant segments with one, two, three and four subdominant trees, respectively. For each projected segment, the CSM is computed on the d values (Fig. 12). The crown of subdominant trees maximally stretches along the z direction (i.e., along the height of the tree). We exploit these characteristics to minimize the local variation of d in the $l-z$ plane, and reduce false peak detection, by using a rectangular spatial filter with the longer side along the z axis. For our dataset, the 6 x 3 rectangular Gaussian filter with $\sigma = 1$ was found to optimal in removing false peaks caused due to locally protruding branch points. The location of a subdominant tree top (red dots in Fig. 13) combined with the nearest valley points on its either (blue dots in Fig. 13) side are used to define the boundary of the subdominant tree. Fig. 13 shows the elliptical boundaries of the subdominant crowns detected in the projected space for cases with one, two, three, and four trees.

The delineation of subdominant tree crowns is performed by exploiting the tree top location, and the 2D crown boundary information modeled from the CSM using the ellipse. The projected space is divided into d_{max}/v voxel layers, where d_{max} is the maximum d value of points in P, and v is the voxel size derived using the semivariogram. Texture segmentation of each voxel slice/layer is done using a marker-controlled watershed algorithm as: a) it allows detecting spatially confined and homogeneous local segments even in the presence of large

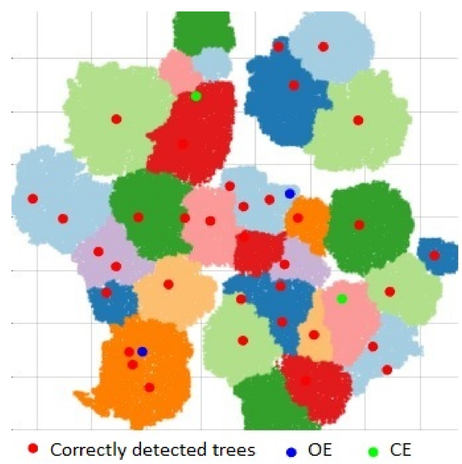

Fig. 8: The candidate tree segments for the plot H1 are shown as color-filled polygons.

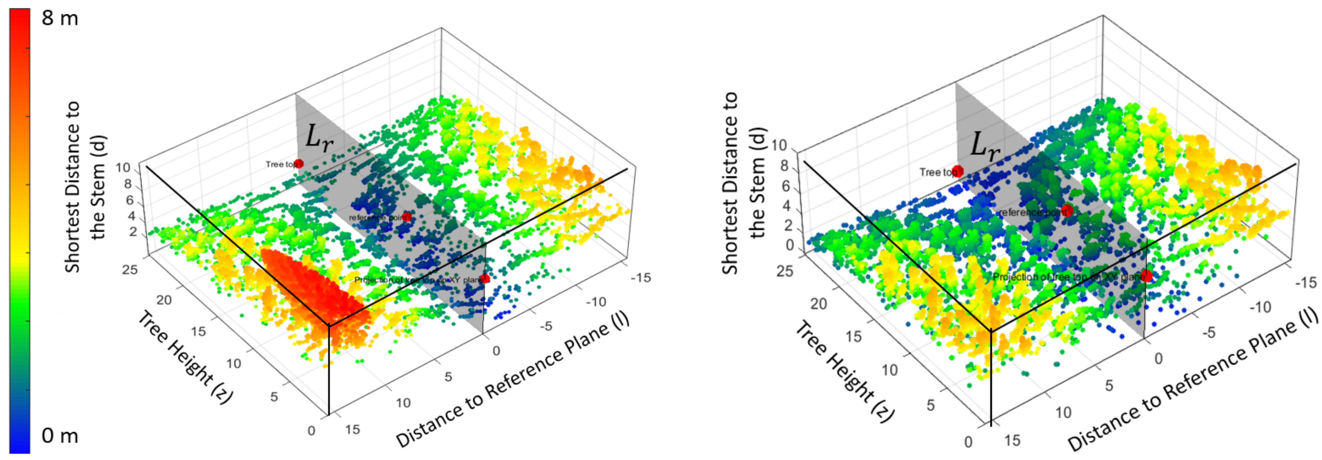

(a) (b)

Fig. 7: Projected point cloud of a 3D candidate tree segment: a) with a subdominant tree, and b) without any subdominant tree.

variance in the data, b) the situation is similar to the case of crown segmentation in a CHM (for which it is largely used), and c) it is simple. Here, the gradient magnitude is used as the segmentation function, the foreground markers are obtained by using the opening-by-reconstruction and the closing-by-reconstruction morphological operations, and the background markers are obtained by considering the watershed ridge lines obtained from the binarization (using Otsu's method [49]) of the original image with the foreground markers superimposed. All segments falling to the subdominant voxel layers and within the respective ellipse are separately stacked to identify the 3D subdominant crown segment(s). Fig. 15 shows the voxel layer segments stacked together to obtain the 3D crown segment of subdominant trees for different subdominant growth situations. All voxel layer interpolated texture feature maps are separately smoothened using the rectangular Gaussian filter with $\sigma = 1$. Point cloud segment of the subdominant tree(s) are obtained by identifying the projected points contained by the 3D voxel set. The mapping to the original space is done using a unique index that is assigned to every data point. Subdominant tree clusters with $t_d < 1.8$ are merged into a single cluster. The value of t_d was obtained using the trial and error method. The objective here was to minimize CE for a set of manually selected 3D candidate segments in the 6 plots for which subdominant crown split occurred.

We compared the proposed method with a point cloud based tree detection and delineation technique, henceforth referred to as the SoA method [36]. The method uses level set analysis on CHM to detect dominant tree apexes, and perform an angular analysis around them to delineate individual crown boundaries. The crown boundary for a tree is derived based on the first local minimum detected on the angular sectors considered around the apex. Further, a sector-wise analysis is performed on the delineated 3D dominant tree segments to detect and delineate any subdominant crown [36]. The dominant and subdominant trees were detected and delineated by employing angular sector-splits of 4 and 8, respectively. The quantization steps for vertical profile analysis is set to 29, and was estimated using the method in [36].

Table II shows the detection accuracies obtained by the proposed method, and the SoA method, for the six sample plots. The proposed method improves the overall detection accuracies by around 5% when compared to the SoA method. The overall accuracy of the proposed tree detection method varies from 88.0% to 96.8% for the six automatically segmented plots. The better performance of the proposed method can be mainly attributed to the projection technique which selectively induces a structural change in dominant tree cloud, thus improving the separability between the dominant and the subdominant cloud segments. This possibility is lacking in the SoA method which is based on a more complex sector-wise analysis that tends to result in tree crown being shared between 3D candidate segments. Thus, the algorithm will identify part of the subdominant crowns in each candidate segment, (and detect it as separate trees) resulting in larger CE (see table II). Whereas, the proposed method minimizes the crown splits by suitably selecting the direction of the reference plane in the projection. The proposed method performs the crown detection analysis in the 3D space, rather than on a projected 2D space as it is the case with the SoA method. Thus it allows the maximum exploration of the structural information in the LiDAR data. For this reason the method can better detect small subdominant trees which are lost when using other methods. Hence reducing the Omission Errors (OE). Fig. 9 shows the histogram of the detected trees by the range of DBH class. The proposed and the SoA method show similar performance for subdominant trees with DBH greater than 40. However, the proposed method was able to detect a larger number of smaller trees (i.e., with DBH less than or equal to 40), when compared to the SoA method. Whatsoever, the performance on detecting trees with DBH less than 20cm is minimum for both the proposed and the SoA methods. This low performance can is attributed to the low point cloud density in lower forest layers. In any case, the proposed method correctly detected a larger number of trees, which proves its effectiveness.

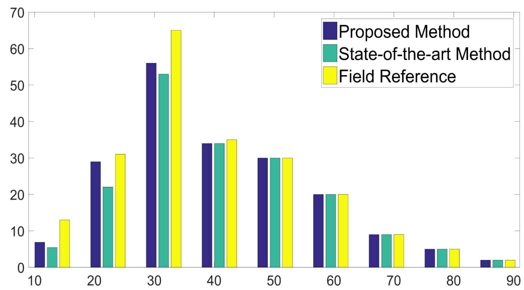

Fig. 9: Overall detection accuracy obtained on the 6 plots, across different DBH classes.

Fig 10 - 16 shows the step-wise mechanism for crown delineation performed on 3D candidate segments of various complexities. It can be seen that the algorithm is able to detect both dominant and subdominant trees for simple (1 tree in the 3D candidate segment) and complex (more than 1 tree in the 3D candidate segment) growth scenarios. The crown delineation performance evaluation was performed on the correctly detected trees. Table. III shows the Mean Error (ME), the Mean Absolute Error (MAE), and the Root Mean Squared Error (RMSE) of the DBH estimates obtained using the proposed, and the SoA method, on the 6 plots. As expected, the proposed method is able to better estimate the DBH of the trees. However, both the proposed and the SoA method underestimate DBH in average. This can be attributed to the low point density in the subdominant layer, and Gaussian smoothing done on the 2D and 3D features. The relatively lower ME, MAE and RMSE provided to the proposed method confirm the average ability of the proposed technique to mitigate the omission errors. The same analysis have been conducted by dividing the dominant-subdominant pairs in 3 groups of delineation complexity defined in terms of proximity among the trees: Group 1 includes the pairs with dominant-subdominant tree distance in the range 0m - 2.5m; Group 2 includes the ones with distance in 2.5m - 5.0m, and Group 3 is the set with pairs of trees being more than 5.0m far from each other. For both the proposed and the SoA method the DBH estimation error is found to be larger for trees with smaller distance (i.e., the ones in $PL1$). However, the proposed approach shows a ME of - 1.80cm which is the 65% of the one achieved by the state of the art. As we move to less complex situations (Groups 1 and 2) the estimation mean error in DBH decreases. This is in accordance with the fact that the crown delineation accuracy improves as the trees are further away from one another, due to smaller overlap. However, the proposed method performs better in these cases as well by resulting in a ME that is less than half the one provided by the SoA method.

IV. Conclusion

In this paper, a novel local projection based tree detection and 3D crown delineation is proposed for high density LiDAR data. The proposed method detects both dominant and sub-dominant trees in multistoried conifer forests. 3D candidate segments are first extracted and then separately analyzed in the projected space to detect and delineate both dominant and subdominant trees. The tree crowns are delineated in 3D by exploiting the projection-induced texture variation extracted using GLCM features. The average crown detection accuracies obtained is 92.3% and the RMSE errors associated with the DBH estimates is 5.13cm. Possible future works include leveraging on the intensity information in LiDAR data, and using datasets with larger point density which include more texture information (e.g., the Terrestrial Laser Scanning data), to improve tree detection and crown delineation.

Acknowledgment

The authors would like to thank the ”Dipartimento Risorse Forestali e Montane” of the Autonomous Province of Trento for providing the high-density LiDAR data used in this study. The data was acquired in the framework of the FORLIDAR project.

References

[1] P. Hyde, R. Dubayah, W. Walker, J. B. Blair, M. Hofton, and C. Hunsaker, “Mapping forest structure for wildlife habitat analysis using multi-sensor (lidar, sar/insar, etm+, quickbird) synergy,” *Remote Sens. Environ.*, vol. 102, no. 1, pp. 63–73, 2006.

[2] S. Magnussen, P. Eggermont, and V. N. LaRiccia, “Recovering tree heights from airborne laser scanner data,” *Forest science*, vol. 45, no. 3, pp. 407–422, 1999.

[3] B. Koch, U. Heyder, and H. Weinacker, “Detection of individual tree crowns in airborne lidar data,” *Photogramm. Eng. Remote Sens.*, vol. 72, no. 4, pp. 357–363, 2006.

[4] J. Peuhkurinen, L. Mehtätalo, and M. Maltamo, “Comparing individual tree detection and the area-based statistical approach for the retrieval of forest stand characteristics using airborne laser scanning in scots pine stands,” *Can. J. For. Res.*, vol. 41, no. 3, pp. 583–598, 2011.

[5] E. Næsset, “Predicting forest stand characteristics with airborne scanning laser using a practical two-stage procedure and field data,” *Remote Sens. Environ.*, vol. 80, no. 1, pp. 88–99, 2002.

[6] J. Holmgren, M. Nilsson, and H. Olsson, “Estimation of tree height and stem volume on plots using airborne laser scanning,” *Forest Science*, vol. 49, no. 3, pp. 419–428, 2003.

[7] L. Duncanson, R. Dubayah, B. Cook, J. Rosette, and G. Parker, “The importance of spatial detail: Assessing the utility of individual crown information and scaling approaches for lidar-based biomass density estimation,” *Remote Sens. Environ.*, vol. 168, pp. 102–112, 2015.

[8] J. Holmgren, Å. Persson, and U. Söderman, “Species identification of individual trees by combining high resolution lidar data with multi-spectral images,” *Int. J. Remote Sens.*, vol. 29, no. 5, pp. 1537–1552, 2008.

[9] A. Persson, J. Holmgren, and U. Söderman, “Detecting and measuring individual trees using an airborne laser scanner,” *Photogramm. Eng. Remote Sens.*, vol. 68, no. 9, pp. 925–932, 2002.

[10] M. Maltamo, K. Mustonen, J. Hyyppä, J. Pitkänen, and X. Yu, “The accuracy of estimating individual tree variables with airborne laser scanning in a boreal nature reserve,” *Can. J. For. Res.*, vol. 34, no. 9, pp. 1791–1801, 2004.

[11] M. Wulder, K. O. Niemann, and D. G. Goodenough, “Local maximum filtering for the extraction of tree locations and basal area from high spatial resolution imagery,” *Remote Sens. Environ.*, vol. 73, no. 1, pp. 103–114, 2000.

[12] A. Kato, L. M. Moskal, P. Schiess, M. E. Swanson, D. Calhoun, and W. Stuetzle, “Capturing tree crown formation through implicit surface reconstruction using airborne lidar data,” *Remote Sens. Environ.*, vol. 113, no. 6, pp. 1148–1162, 2009.

TABLE II: Detection accuracy (DET), commission error (CE) and omission error (OE) obtained with the proposed and SoA methods.

Plot ID	Trees	Proposed Method			State-of-the-art Method		
		DET	CE	OE	DET	CE	OE
H1	40	38 (95.0%)	2 (5.0%)	2 (5.0%)	35 (87.5%)	4 (10.0%)	5 (12.5%)
H2	32	31 (96.8%)	1 (3.0%)	1 (3.0%)	29 (90.0%)	3 (9.3%)	3 (9.3%)
H3	30	27 (90.0%)	2 (6.6%)	3 (10.0%)	28 (93.3%)	4 (13.3%)	2 (6.6%)
H4	25	22 (88.0%)	2 (8.0%)	3 (12.0%)	21 (84.0%)	2 (8.0%)	3 (12.0%)
H5	45	40 (88.8%)	3 (6.6%)	5 (11.1%)	38 (84.4%)	3 (6.6%)	7 (15.5%)
H6	38	36 (94.7%)	3 (7.8%)	2 (5.2%)	33 (86.8%)	4 (10.5%)	5 (13.1%)
Total	210	194 (92.3%)	13 (6.1%)	16 (7.6%)	184 (87.6%)	20 (9.5%)	25 (11.9%)

TABLE III: The ME, the MAE, and the RMSE accuracy of estimated DBH for the proposed and the state-of-the-art method.

Method	ME	MAE	RMSE
Proposed	-0.12 cm	3.91 cm	5.13 cm
SoA	-0.55 cm	4.34 cm	5.62 cm

TABLE IV: The ME, the MAE, and the RMSE accuracy of estimated DBH for the proposed and the state-of-the-art method by delineation complexity.

Dominant to Subdominant Distance	Method	ME	MAE	RMSE
Group 1 (0.0-2.5 m)	Proposed	-1.80 cm	5.20 cm	6.80 cm
	SoA	-2.80 cm	5.60 cm	6.90 cm
Group 2 (2.5-5.0 m)	Proposed	-0.15 cm	3.88 cm	4.91 cm
	SoA	-0.83 cm	4.60 cm	5.80 cm
Group 3 (> 5.0m)	Proposed	-0.30 cm	4.90 cm	6.20 cm
	SoA	-0.90 cm	5.40 cm	6.60 cm

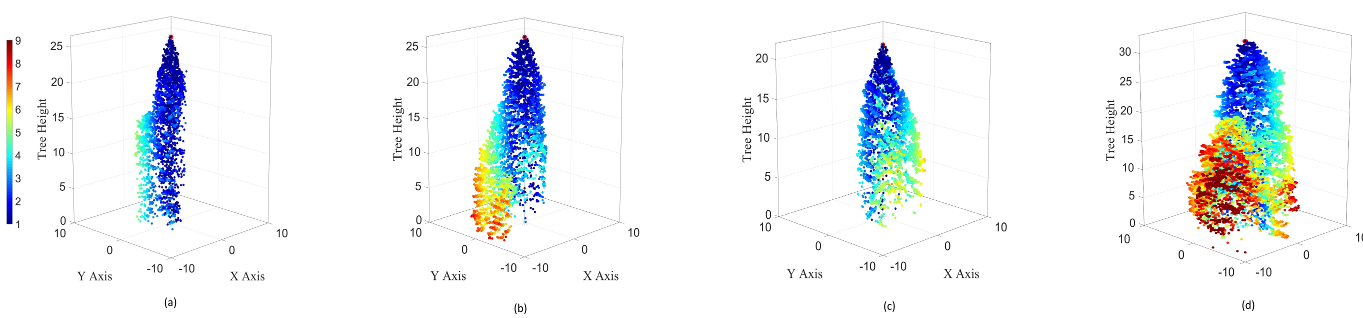

Fig. 10: Point cloud of 3D candidate segments in the original space with: (a) one, (b) two, (c) three, and (d) four subdominant trees. The colorbar shows the distance of a point to the projection axis.

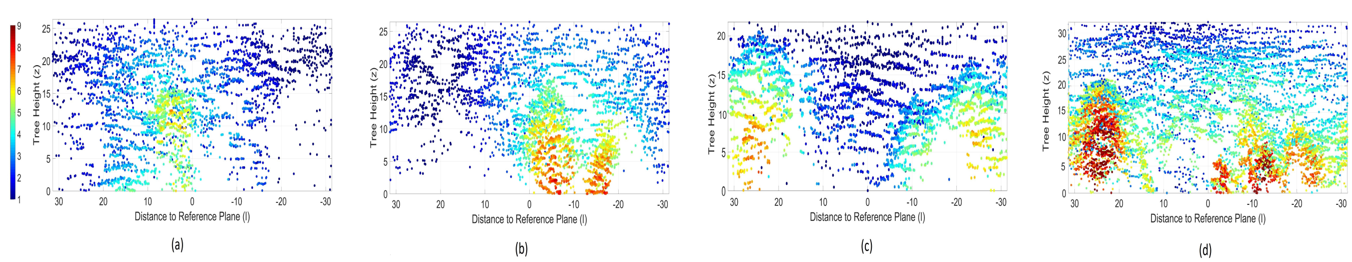

Fig. 11: Projected point cloud of the 3D candidate segment with: (a) one, (b) two, (c) three, and (d) four subdominant trees.

[13] T. Brandtberg, T. A. Warner, R. E. Landenberger, and J. B. McGraw, "Detection and analysis of individual leaf-off tree crowns in small footprint, high sampling density lidar data from the eastern deciduous forest in north america," *Remote Sens. Environ.*, vol. 85, no. 3, pp. 290–303, 2003.

[14] A. Khosravipour, A. K. Skidmore, and M. Isenburg, "Generating spike-

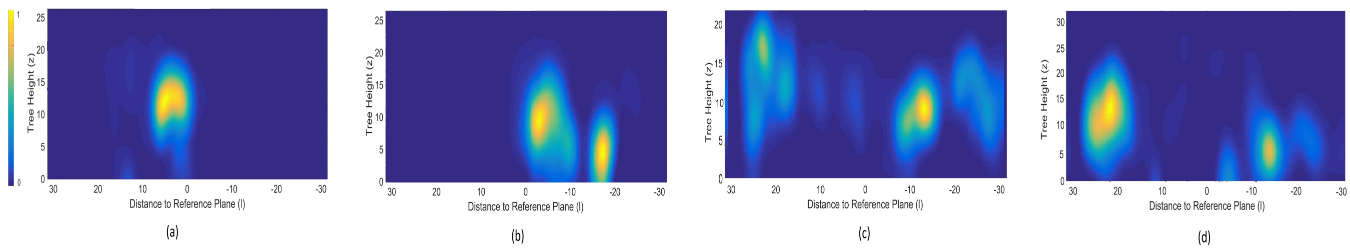

Fig. 12: The CSSM map derived from the projected 3D candidate segment data with: (a) one, (b) two, (c) three, and (d) four subdominant trees.

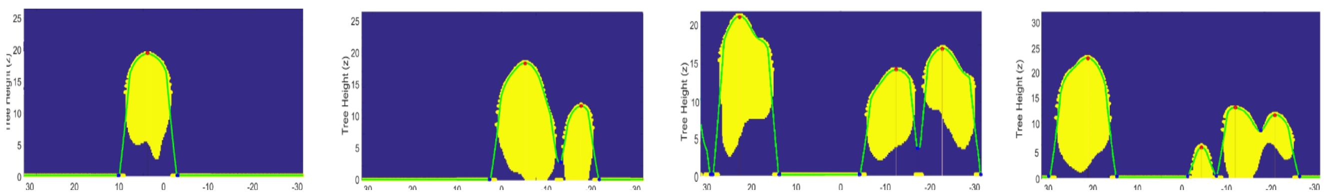

Fig. 13: The segmented projected 3D candidate segment map with: (a) one, (b) two, (c) three, and (d) four subdominant trees. The local maxima (red dots) and local minima (blue dots) derived from the foreground segment (yellow) are used to define the elliptical boundary.

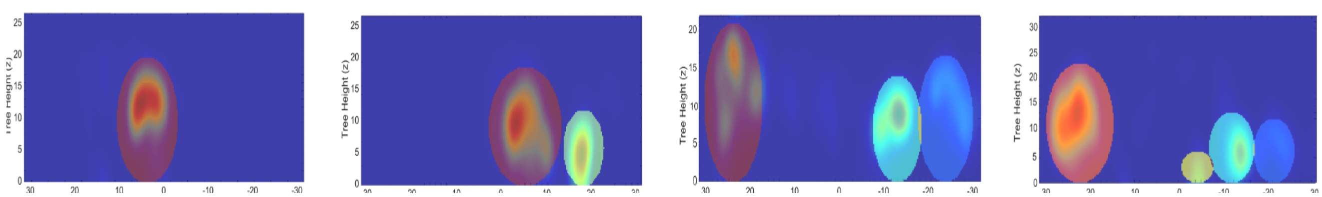

Fig. 14: Elliptical tree crown boundary obtained on the projected 3D candidate segment map binary images with: (a) one, (b) two, (c) three, and (d) four subdominant trees. The elliptical crown boundaries derived from CSM for subdominant trees are shown in unique colors.

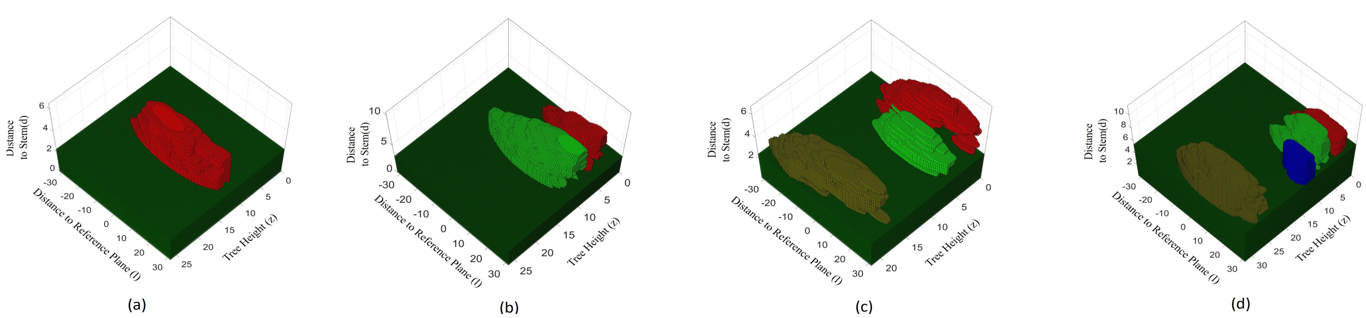

Fig. 15: Stacked segments from different voxel layers for: (a) one, (b) two, (c) three, and (d) four subdominant trees.

free digital surface models using lidar raw point clouds: A new approach for forestry applications," *Int. J. Appl. Earth Obs. Geoinf.*, vol. 52, pp. 104–114, 2016.

[15] B.-M. Straub and C. Heipke, "Concepts for internal and external evaluation of automatically delineated tree tops," *Int. Arch. Photogramm. Remote Sens.*, vol. 26, no. 8/W2, pp. 62–65, 2004.

[16] H. Weinacker, B. Koch, U. Heyder, and R. Weinacker, "Development of filtering, segmentation and modelling modules for lidar and multispectral data as a fundament of an automatic forest inventory system," *Int. Arch. Photogramm. Remote Sens. Spat. Inf. Sci..*, vol. 36, no. Part 8, p. W2, 2004.

[17] S. C. Popescu and R. H. Wynne, "Seeing the trees in the forest," *Photogrammetric Engineering & Remote Sensing*, vol. 70, no. 5, pp. 589–604, 2004.

[18] D. Tiede and C. Hoffmann, "Process oriented object-based algorithms for single tree detection using laser scanning," in *Workshop on 3D Remote Sensing in Forest*, 2006, pp. 14–15.

[19] J. P. Ardila, W. Bijker, V. A. Tolpekin, and A. Stein, "Context-sensitive extraction of tree crown objects in urban areas using vhr satellite images," *Int. J. Appl. Earth Obs. Geoinf.*, vol. 15, pp. 57–69, 2012.

[20] F. Morsdorf, E. Meier, B. Allgöwer, and D. Nüesch, "Clustering in airborne laser scanning raw data for segmentation of single trees," *Int.*

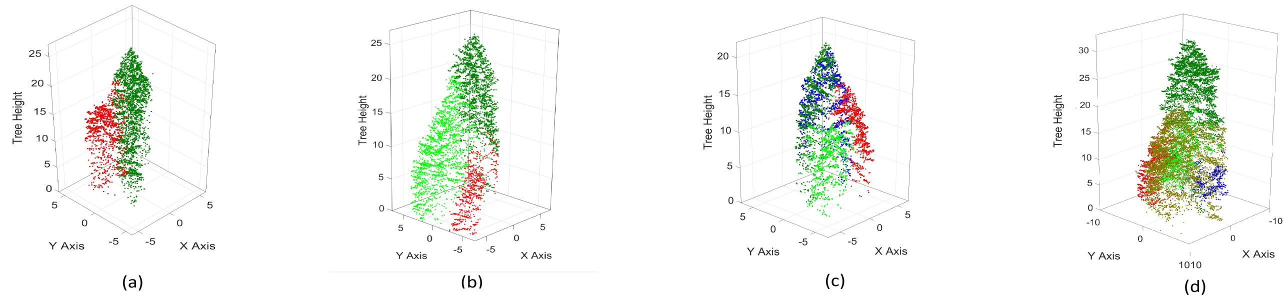

Fig. 16: The tree point cloud segments for: (a) one, (b) two, (c) three, and (d) four subdominant trees.

Arch. Photogramm. Remote Sens. Spat. Inf. Sci., vol. 34, no. part 3, p. W13, 2003.

[21] H. Lee, K. C. Slatton, B. Roth, and W. Cropper Jr, "Adaptive clustering of airborne lidar data to segment individual tree crowns in managed pine forests," *Int. J. Remote Sens.*, vol. 31, no. 1, pp. 117–139, 2010.

[22] W. Li, Q. Guo, M. K. Jakubowski, and M. Kelly, "A new method for segmenting individual trees from the lidar point cloud," *Photogramm. Eng. Remote Sens.*, vol. 78, no. 1, pp. 75–84, 2012.

[23] L. Duncanson, B. Cook, G. Hurtt, and R. Dubayah, "An efficient, multi-layered crown delineation algorithm for mapping individual tree structure across multiple ecosystems," *Remote Sens. Environ.*, vol. 154, pp. 378–386, 2014.

[24] H. Hamraz, M. A. Contreras, and J. Zhang, "Forest understory trees can be segmented accurately within sufficiently dense airborne laser scanning point clouds," *Sci. Rep.*, vol. 7, no. 1, p. 6770, 2017.

[25] E. Ayrey, S. Fraver, J. A. Kershaw Jr, L. S. Kenefic, D. Hayes, A. R. Weiskittel, and B. E. Roth, "Layer stacking: a novel algorithm for individual forest tree segmentation from lidar point clouds," *Can. J. For. Res.*, vol. 43, no. 1, pp. 16–27, 2017.

[26] Y. Wang, H. Weinacker, and B. Koch, "Development of a procedure for vertical structure analysis and 3d-single tree extraction within forests based on lidar point cloud," *Int. Arch. Photogramm. Remote Sens. Spat. Inf. Sci.*, vol. 36, no. Part 3, p. W52, 2007.

[27] D. Mongus and B. Žalik, "An efficient approach to 3d single tree-crown delineation in lidar data," *ISPRS J. Photogramm. Remote Sens.*, vol. 108, pp. 219–233, 2015.

[28] H. Kaartinen, J. Hyyppä, X. Yu, M. Vastaranta, H. Hyyppä, A. Kukko, M. Holopainen, C. Heipke, M. Hirschmugl, F. Morsdorf *et al.*, "An international comparison of individual tree detection and extraction using airborne laser scanning," *Remote Sensing*, vol. 4, no. 4, pp. 950–974, 2012.

[29] J. Vauhkonen, L. Ene, S. Gupta, J. Heinzel, J. Holmgren, J. Pitkänen, S. Solberg, Y. Wang, H. Weinacker, K. M. Hauglin *et al.*, "Comparative testing of single-tree detection algorithms under different types of forest," *Forestry*, vol. 85, no. 1, pp. 27–40, 2012.

[30] J. Reitberger, C. Schnörr, P. Krzystek, and U. Stilla, "3d segmentation of single trees exploiting full waveform lidar data," *ISPRS J. Photogramm. Remote Sens.*, vol. 64, no. 6, pp. 561–574, 2009.

[31] Y. Wang, H. Weinacker, B. Koch, and K. Sterenczak, "Lidar point cloud based fully automatic 3d single tree modelling in forest and evaluations of the procedure," *Int. Arch. Photogramm. Remote Sens. Spat. Inf. Sci.*, vol. 37, no. PART B6B, pp. 45–51, 2008.

[32] C. Véga, A. Hamrouni, S. El Mokhtari, J. Morel, J. Bock, J.-P. Renaud, M. Bouvier, and S. Durrieu, "Ptrees: A point-based approach to forest tree extraction from lidar data," *Int. J. Appl. Earth Obs. Geoinf.*, vol. 33, pp. 98–108, 2014.

[33] X. Lu, Q. Guo, W. Li, and J. Flanagan, "A bottom-up approach to segment individual deciduous trees using leaf-off lidar point cloud data," *ISPRS J. Photogramm. Remote Sens.*, vol. 94, pp. 1–12, 2014.

[34] C. D. Jones, A. B. Smith, and E. F. Roberts, in *Proceedings Title*, vol. II. IEEE, 2003, pp. 803–806.

[35] E. Lindberg, L. Eysn, M. Hollaus, J. Holmgren, and N. Pfeifer, "Delineation of tree crowns and tree species classification from full-waveform airborne laser scanning data using 3-d ellipsoidal clustering," *IEEE J. Sel. Top. Appl. Earth Obs. Remote Sens.*, vol. 7, no. 7, pp. 3174–3181, 2014.

[36] C. Paris, D. Valduga, and L. Bruzzone, "A hierarchical approach to three-dimensional segmentation of lidar data at single-tree level in a multilayered forest," *IEEE Trans. Geosci. Remote Sens.*, vol. 54, no. 7, pp. 4190–4203, 2016.

[37] M. Maltamo, T. Tokola, and M. Lehikoinen, "Estimating stand characteristics by combining single tree pattern recognition of digital video imagery and a theoretical diameter distribution model," *Forest Science*, vol. 49, no. 1, pp. 98–109, 2003.

[38] L. Mehtätalo, "Eliminating the effect of overlapping crowns from aerial inventory estimates," *Can. J. For. Res.*, vol. 36, no. 7, pp. 1649–1660, 2006.

[39] K. Kansanen, J. Vauhkonen, T. Lähivaara, and L. Mehtätalo, "Stand density estimators based on individual tree detection and stochastic geometry," *Can. J. For. Res.*, vol. 46, no. 11, pp. 1359–1366, 2016.

[40] J. Vauhkonen and L. Mehtätalo, "Matching remotely sensed and field-measured tree size distributions," *Can. J. For. Res.*, vol. 45, no. 3, pp. 353–363, 2014.

[41] T. Lahivaara, A. Seppanen, J. P. Kaipio, J. Vauhkonen, L. Korhonen, T. Tokola, and M. Maltamo, "Bayesian approach to tree detection based on airborne laser scanning data," *IEEE Trans. Geosci. Remote Sens.*, vol. 52, no. 5, pp. 2690–2699, 2014.

[42] P. Neubert and P. Protzel, "Compact watershed and preemptive slic: On improving trade-offs of superpixel segmentation algorithms," in *Pattern Recognition (ICPR), 2014 22nd International Conference on*. IEEE, 2014, pp. 996–1001.

[43] A. Harikumar, F. Bovolo, and L. Bruzzone, "A novel approach to internal crown characterization for coniferous tree species classification," in *SPIE Remote Sensing*. International Society for Optics and Photonics, 2016, pp. 100 040H–100 040H.

[44] C. Philips, D. Li, D. Raicu, and J. Furst, "Directional invariance of co-occurrence matrices within the liver," in *Biocomputation, Bioinformatics, and Biomedical Technologies, 2008. BIOTECHNO'08. International Conference on*. IEEE, 2008, pp. 29–34.

[45] R. M. Haralick, K. Shanmugam *et al.*, "Textural features for image classification," *IEEE Trans. Syst. Man Cybern. Part B Cybern.*, no. 6, pp. 610–621, 1973.

[46] P. Li and X. Xiao, "An unsupervised marker image generation method for watershed segmentation of multispectral imagery," *Geosciences Journal*, vol. 8, no. 3, pp. 325–331, 2004.

[47] K. Olofsson, E. Lindberg, J. Holmgren *et al.*, "A method for linking field-surveyed and aerial-detected single trees using cross correlation of position images and the optimization of weighted tree list graphs," *Proceedings of SilviLaser*, vol. 2008, p. 8th, 2008.

[48] J. Kalliovirta and T. Tokola, "Functions for estimating stem diameter and tree age using tree height, crown width and existing stand database information," *Silva Fennica*, vol. 39, no. 2, pp. 227–248, 2005.

[49] N. Otsu, "A threshold selection method from gray-level histograms," *IEEE transactions on systems, man, and cybernetics*, vol. 9, no. 1, pp. 62–66, 1979.